COMPUTATIONAL/EXPERIMENTAL ANALYSIS OF THREE LOW SONIC BOOM CONFIGURATIONS WITH DESIGN MODIFICATIONS

Susan E.Cliff
NASA Ames Research Center
Moffett Field, CA

SUMMARY

The Euler code, designated AIRPLANE, which uses an unstructured tetrahedral mesh was used to compute near-field sonic boom pressure signatures on three modern low sonic boom configurations: the Mach2 , Mach3, and Haglund models. The TEAM code which uses a multi-zoned structured grid was used to calculate pressure signatures for the Mach2 model. The computational pressure signatures for the Mach2 and Mach3 models are compared with recent experimental data. The computed pressure signatures were extracted at distances less than one body length below the configuration and extrapolated to the experimental distance. The Mach2 model was found to have larger overpressures off-ground-track than on-ground-track in both computational and experimental results. The correlations with the experiment were acceptable where the signatures were not contaminated by instrumentation and model-support hardware. AIRPLANE was used to study selected modifications to improve the overpressures of the Mach2 model.

INTRODUCTION

Low sonic boom levels for the next generation supersonic civil transports are necessary if supersonic flight over populated areas is permitted. Three modern low boom configurations have been designed with "shaped" pressure signatures. The Mach2 model (ref. 1) and the Haglund model (ref. 2) were designed to have "flat-top" pressure signatures, whereas the Mach3 model (ref 1) was designed to have a "ramped" pressure signature on the ground. This was not achieved with the inadequate length of the ramped portion of the area distribution. These models have been designed primarily using quasi-linear methods. The approach of this research is to use Euler codes to predict sonic boom for comparison with experimental data. The CFD pressure signatures are taken close to the model so that sufficient grid densities can be maintained and then extrapolated to greater distances. Euler and Potential methods have been shown to give good correlations with experiment for three generic configurations (refs. 3,4,5).

Recent Euler analyses of the Mach2 and Mach3 models by Siclari and Darden (ref. 6) have indicated significant off-ground-track sonic boom levels in comparison with the level on-ground-track. This was

verified experimentally in the Ames 9x7-Foot Supersonic Wind Tunnel, as well as computationally using the AIRPLANE code. Suggested modifications to the Mach2 configuration are included in this study which reduce the shock strengths off-ground-track without significantly changing the signature directly below the model. Increasing the leading edge sweep of the outboard wing panel was found to reduce the strength of the off-ground-track shocks without adversely affecting on-track pressures. The effects of using non-linear dihedral, which increases towards the wing tips, were also investigated with AIRPLANE.

APPROACH

Two Euler finite volume codes were used: AIRPLANE and Three dimensional Euler/Navier-Stokes Aerodynamic Method (TEAM). AIRPLANE consists of two programs: MESHPLANE and FLOPLANE, the grid generator and the flow solver, respectively. These programs were developed by Baker and Jameson to model complex configurations using unstructured grids. MESHPLANE generates the tetrahedra using a method based on Delaunay triangulation (refs. 7,8, and 9). Interior points placed approximately normal to the surface adjacent to each surface point are triangulated along with the surface points to improve the surface triangulation and to distinguish surface triangles from flow field triangles. The method is constrained such that the surface is not altered when exterior points near the surface of the configuration are triangulated. The points that lie within the interior of the configuration are deleted during the volume triangulation. The laborious procedure of blocking and gridding structured multiple-zone grids is eliminated by AIRPLANE. The flow solver FLOPLANE uses a finite volume algorithm that computes flow variables at the vertices of each tetrahedron (ref. 10).

The Euler solver in TEAM is an enhanced version of Jameson's cell-centered FLO57 (ref. 11). Raj et al. added the Navier-Stokes capability, several dissipation schemes, residual smoothing, and boundary conditions which can model specified mass flow ratios (ref. 12). TEAM has the ability to use structured blocked grids of arbitrary topology without one-to-one grid abutments. A multiple zoned structured grid was generated using the General Dynamics GRIDGEN programs (ref. 13). The surface grid was generated using a CAD/CAM system. The flow-field grid was generated using GRIDGEN programs. The block structure and edge point distributions were developed using GRIDBLOCK. The faces of each block were generated using the algebraic or elliptic solvers in GRIDGEN2D. The volume grid was generated by GRIDGEN3D using the algebraic solvers.

Comparisons of experimental pressure signatures with extrapolated computational near-field Euler pressure signatures for three modern low boom configurations are presented. The experimental pressure signatures for the Mach2 and Mach3 models were measured at distances ranging from approximately one

half to two body lengths below the model. Obtaining computational data at half a body length was found to be difficult with the current CFD methods due to the large computer resources required to maintain dense grids away from the body. In addition to grid density, the dissipation inherent in the numerical procedure required to improve convergence causes rapid shock strength decay with increasing distance from the configuration. To obtain accurate solutions, most CFD data used in this study were extracted at a quarter body length and then extrapolated to the experimental distance. The extrapolation code used for this study is a waveform parameter method based on geometric acoustics for the wave amplitude and isentropic theory for the non-linear waveform distortions (ref. 14).

A photograph of the Mach 2 model installed in the wind tunnel is shown in Figure 1. An external strain gage is visible on the sting downstream of the model base. Fore and aft sections of the model are held together by screws located ahead of the vertical tail. The screw holes were filled with plaster before testing. The nacelles were made of fiber-glass and were removable. A planform view showing the upper surface of the Mach3 model is shown in Figure 2. Note the sharp nose of the fuselage, designed to produce a ramped (finite rise) pressure signature. An isometric view of the Haglund model showing the computational surface grid shaded by the surface normals is shown in Figure 3. The design goals of the Haglund model were to have a "flat-top" pressure signature on the ground at Mach 1.7 and for a flight altitude of 44,000 feet.

MACH2 MODEL

Computational Grids - Mach2 Model

TEAM grid

The TEAM computation for the Mach2 model with pylons, flow-through nacelles, and vertical tail at M=2.00, α=0° was obtained using a 78-zone grid. The grid was swept 30° from the freestream direction to maintain grid density and improve shock capturing in the flow-field. The upstream boundary was placed 1.5 body lengths ahead of the model, the downstream boundary was 6.0 body lengths from the nose of the model, whereas the vertical and spanwise boundaries were 4.0 body lengths from the model. The block boundaries of the computational grid on the upper surface are shown in Figure 4. The grid consisted of 1,850,084 points. Note that the abutment lines on the surface are for the most part parallel to the free-stream direction. A grid which uses a spanwise definition is preferred when the wing sweep exceeds 45°, but in order to model the pylons and nacelles accurately a compromise in grid quality was selected. The 2:1 abutment capability in TEAM can greatly reduce the number of grid points. For example, the fuselage used 101 points in the streamwise direction, while the wing had 35 points on the tip. The grid had 118 and 91 points in the vertical and spanwise directions, respectively. A view of the flow-through nacelles is shown in

Figure 5. Note that the chamfered faces of the nacelles are modeled and that the block faces are colored differently. The 2:1 abutments on the wing lower surface can be seen where the green, and cyan blocks meet and where the blue and yellow blocks abut.* A view of the block structure on the interior and exterior of the nacelles at the inlet face is shown in figure 6. The nacelles are enclosed in a rectangular grid, with the faces of the blocks colored differently. The nacelles required approximately 40 of the 78 blocks of grid.

AIRPLANE grid

The symmetry plane of the tetrahedral mesh used with AIRPLANE is illustrated in Figures 7a-7c. The upstream boundary was placed near the model nose since upstream influence should not exist at supersonic Mach numbers. The staging of mesh densities through a sequence of nested lattices is evident in these figures. Each stage represents a 2:1 grid refinement. Red and green boxes enclose regions of differing grid densities and the final view shows the surface grid in the symmetry plane; note that the model supporting sting used in experiment was included in the computations. A total of 259,121 mesh points, 1,555,988 volume tetrahedra and 13,692 surface triangles were used for the configuration with nacelles.

A partial view of the lower surface grid of the Mach2 model is shown in Figure 8. Note that nacelles are open allowing flow to pass through. The surface grid points used with TEAM were used as input into MESHPLANE for surface triangulation and subsequent tetrahedral volume griding. This was not ideal, but was the only surface definition available at the time, a spanwise definition would improve the surface triangulation, particularly along the leading edge of the wing.

Computational Results - Mach2 Model

The TEAM pressure signatures for the Mach2 model with flow through nacelles are compared with experimental data at Mach 2.0 and an angle of attack of 0.0° in Figure 9. The TEAM pressure signature was obtained at 0.2 body lengths from the model and extrapolated to a distance of 1.085 body lengths. Note that the bow shock strength predicted by TEAM is less than experiment and smeared. This may be due to insufficient grid density in the region of the bow shock. However, the magnitude of the flat portion of the pressure signature is fairly accurately predicted. The strong shock due the blunt lips of the nacelles is predicted by TEAM. The nacelles were unstarted during the wind tunnel test and would be expected to produce a stronger shock than the flow through nacelles modeled in the computations. The Euler computations indicate that the blunt lips are primarily responsible for the large nacelle shock strength.

The AIRPLANE computation with flow-through nacelles is shown in Fig 10. The bow shock and flat top region of the signature is more accurately predicted by AIRPLANE than TEAM. The strength of the nacelle shock is lower for AIRPLANE than TEAM; however, the actual shock strength with started nacelles

*Figures are not shown in color.

is unknown. The unstructured grid code is better suited to complex configurations, because regions of poor grid quality often encountered when a structured grid is used are avoided. The series of shock waves downstream of the tail shock are associated with instrumentation and model support hardware and were not included in the computations. Further discussion of this issue will be presented in the Mach3 model section of this report.

The Mach2 model was also tested without nacelles. A comparison of an extrapolated AIRPLANE pressure signature directly below the model with wind tunnel data from the Ames 9x7-Foot Supersonic Wind Tunnel is shown in Fig 11. The correlation with experiment is good, but the bow shock is slightly smeared. In this case the aft portion of the signature which was corrupted by model support hardware was deleted. In addition to the on-ground-track pressure signature, a signature at an azimuthal angle of 45°was also measured. The off-ground-track pressure spike initially predicted by Siclari and Darden was validated both computationally, with AIRPLANE, and experimentally (Fig 12). AIRPLANE again underpredicts the strength of the bow shock, but the overall shape of the signature and difference in magnitudes of the bow and outboard wing shock are well predicted by AIRPLANE.

AIRPLANE used about 10 CPU hours and 90 million words of memory on the Cray 2. TEAM used approximately 8 hours of CPU time and 8 million words of memory on the Cray Y-MP. The AIRPLANE computations for the models discussed below used approximately the same memory and CPU time per grid point as the Mach2 model.

MACH 3 MODEL

Computational Grids - Mach3 Model

AIRPLANE grid

The fuselage of the Mach3 model was defined using sections perpendicular to the free stream, resulting in a more accurate nose definition. The tail and most of the wing were defined using streamwise cross sections. The outer wing near the tip used sections parallel to the trailing edge in order to accurately model the leading edge in this region. Grids for the model were developed with and without nacelles. The pylons were not modeled since they were assumed insignificant to the sonic boom computations. The nacelles were modeled with solid faces to simulate unstart. The upstream and downstream faces were defined with a center point and two concentric circles between the center and the exterior of the nacelles. The exterior surface of the nacelles were modeled using circular sections normal to the axis of each nacelle.

The lower surface grid near the nacelles is shown in Figure 13. A total of 230,537 mesh points, 1,367,809 volume tetrahedra, and 12,735 surface triangles were used to compute the flow about the configuration with nacelles.

Computational Results - Mach3 Model

Computational pressure signatures for the Mach 3 model with and without nacelles were obtained with AIRPLANE. This configuration was tested at Mach numbers of 2.50 in the Ames 9x7- and the Langley 4x4-Foot Supersonic Wind Tunnels. The Mach 2.96 data was obtained in the Langley 4x4-Foot Supersonic Wind Tunnel.

The pressure signatures obtained with AIRPLANE and the experimental data for Mach 2.50, h/l = 0.47, C_L = 0.072 are shown in Figure 14. The computational data were obtained at a distance of 0.25 body lengths and extrapolated to the experimental altitude. The forward portion of the signature is accurately predicted. However, the correlation for the aft portion is poor. Schlieren photography was used to investigate the cause of the multiple shocks in the aft portion of the experimental signature. The Mach2 and Mach3 models were built in two pieces and attached with screws located upstream of the vertical tail (Figures 1 and 2). The screw holes were filled with dental plaster during testing. The plaster was sanded, yielding a non-smooth surface which may be responsible for the series of weak shocks shown near the model base in figure 15. Also, an external strain gage attached to the sting downstream of the model base generates additional shock waves. These shock waves can be seen by careful examination of the Schlieren photography of figures 15 and 16. The adapter connecting the sting to the angle of attack mechanism generates additional shock waves, as does the shroud covering of the strain gage wires. The angle of attack mechanism was placed approximately one body length behind the model. The strong shocks emanating from the angle of attack mechanism begin corrupting the signatures at distances of approximately one body length and greater at Mach 2.50. The coalescence of shocks from the angle of attack mechanism and the adapter can be seen in Figure 17. The experimental pressure signature at h/l = 0.94 is compared with an AIRPLANE signature extrapolated from h/l =0.25 to 0.94 and Langley 4x4-Foot experimental data extrapolated from h/l = 0.47 to 0.94 (Figure 18). The extrapolated experimental signature and the extrapolated computational data do not correlate well in the region of the second expansion at h/l = 0.94. The reason for this is not well understood at this time but may be related to three-dimensional effects which may not be affecting the centerplane at the closer altitudes of experiment and the computations, and to shocks emanating from the filled screw holes. The forward portion of the computational signature correlates better with the experimental data than for an h/l of 0.47 (compare Figures 14 and 18). Note, in particular, that the correlation for the bow shock is better at h/l = 0.94 than at h/l = 0.47, probably due to smearing of both CFD and experiment. The strong shock at the rear of the experimental pressure signature is due to the angle of attack mechanism. A similar shock is observed in the computations because the entire sting including the ramped portion which joins the adapter to the angle of attack mechanism was modeled.

The computations with blocked nacelles compared with experimental data from the 9x7-Foot Supersonic Wind Tunnel are shown in Figures 19a - 19c. The computations were extracted at an h/l of 0.2 and extrapolated to an h/l of 0.68. The Mach3 model was tested at Mach 2.5, the maximum Mach number of the 9x7-Foot Supersonic Wind Tunnel. The correlation with experiment is excellent at an h/l of 0.68. The magnitude of the shock due to the unstarted nacelles is well predicted by AIRPLANE. The experimental data downstream of the nacelle was contaminated by interference from the angle of attack mechanism and is not shown. The correlation at one body length is also good. Note that the computational lift coefficient is greater than the experimental lift coefficient in figures 19a and 19b and that good correlation is obtained. The computational lift coefficient shown in figure 19c is less than the experimental value and the correlation with experiment is poorer. The lower angle of attack used with the inviscid Euler code to obtain the desired lift coefficient results in weaker shocks, therefore the computational lift coefficient must be greater than experiment for improved signature correlation.

Pressure signatures for the Mach3 model were also computed at its design Mach number and compared with Langley 4x4-Foot Supersonic Wind Tunnel data and with computations by Siclari and Darden (ref. 6, Figure 20a.). The lift coefficient of the Siclari-Darden computation were not given in ref. 6, but is assumed to be less than experiment. The forward portion of the AIRPLANE pressure signature correlates well with the experimental data as observed in previous computations. The two Euler codes predict similar pressure signatures with the same number of shocks and expansions. The series of weak shocks shown in the wind tunnel data is not observed in the computations because the external gages, adapter, irregular shroud over the adapter, and angle of attack mechanism were not modeled. An computational/experimental comparison at an altitude of 0.94 body lengths is shown in Figure 20b. Again, poor correlation in the aft region of the signature is observed. Coalescence of shocks from the model support hardware with model shocks occurs closer to the model at higher Mach numbers. The strong shock in the aft region of the experimental signature is due to the coalescence of the model tail and the angle of attack mechanism shocks.

HAGLUND MODEL

Computational Grids - Haglund Model

The wing/body portion of the computational Haglund model was defined by sections normal to free-stream. This gave a more accurate triangulation of the highly swept leading edge of the wing. An isometric view of the computational model showing the surface triangulation is shown in figure 21. The number of

points for each defining section increased from the nose, defined by a single point, to the sections near the wing tip which had 136 points. The trailing edge of the wing tip is also defined with a single point. The spanwise sections near the tip do not include the sting. The thin wing tip required only upper and lower surface points to define the section at the wing tip. The configuration without nacelles was defined with two components, the wing/body and the sting. A total of 344,043 mesh points, 2,110,627 volume tetrahedra, and 4,655 surface triangles were used to compute the flow about the configuration without nacelles.

The complete Haglund configuration with nacelles and diverters was modeled computationally. The nacelles are in close proximity to the wing and are canted downward to minimize boundary layer interaction with the inlet and to align the inlet with the local flow direction. A small section of the inboard nacelles near the trailing edge of the wing protruded through the upper surface of the wing in the CAD definition, requiring lowering of the nacelles to a allow adequate grid points on the diverter. The internal portion of the nacelle was modeled such that the cross sectional area was held constant. This results in a blunt base on the nacelle and was chosen to insure that the flow does not expand or compress inside the nacelle, thus preventing a drag error. The drag due to the blunt base of the nacelle must be subtracted from the total drag. The nacelles and diverters required very fine grid spacing in the streamwise direction which increases in density at the rear of the diverter. The wing maintains this dense region of grid points which should ensure shock capture for the nacelles. The nacelles and diverters were defined using streamwise cross-sections. An isometric view of the upper surface of the configuration is shown in figure 22. A view of the lower surface showing the nacelles and diverters is shown in figure 23. A total of 437,672 mesh points, 2,666,437 volume tetrahedra, and 27,972 surface triangles were used to compute the flow about the complete configuration.

Computational Results - Haglund Model

The AIRPLANE pressure signatures for the Haglund Model without nacelles were computed at Mach 1.7 and $\alpha = 4.5°$, which produced a lift coefficient of 0.091, slightly above the cruise value of 0.085. The computational pressure signatures at distances of 0.20 and 0.40 body lengths are shown in Fig 24. Both signatures show rough approximations of a "flat-top" pressure signature. The signature is not as flat as the Mach2 model signature, but the configuration is more apt to meet its mission requirements. The highly swept, cambered and twisted arrow wing distributes the lift along the length of the configuration, thereby separating the shock waves and reducing their magnitude so that shock coalescence is minimized.

The pressure signature of the Haglund model with nacelles and diverters modeled at distances of 0.2 and 0.40 body lengths is shown in Figure 25. This solution was obtained at a lower angle of attack ($\alpha = 4°$ as opposed to 4.5°) than for the isolated wing case, to allow for the lift due to the nacelles. The lift due to the nacelles was overestimated and a computational lift coefficient of 0.081 was obtained. The strong shock

emanating from the nacelle/diverter is clearly evident in the pressure signatures at 0.2 body lengths, but the shock is narrow and dissipates rapidly as shown in the signatures at 0.4 body lengths. The nacelles appear to have improved the pressure signature; the second expansion is minimized resulting in a more flat top signature. Upon extrapolation of the pressure signatures to the ground, multiple weak shocks in the "flat-top" region of the signature were obtained.

DESIGN MODIFICATIONS - MACH2 MODEL

The first design modifications applied to the Mach2 model were to increase the leading edge sweep of the outboard portion of the wing from 52° to 62° and then to 70° in an attempt to reduce the off-ground-track overpressures. The increase in sweep was achieved by shearing the wing sections in the streamwise direction to maintain area and aspect ratio as nearly as possible. The original sweep of 52° resulted in a supersonic leading edge for the outboard wing panel which was assumed to be responsible in part for the unacceptable off-track pressures. Another attempt to alleviate the off-track pressures was to reduce the cruise Mach number of the configuration to Mach 1.6. This was found to be unsuccessful; the large sweep change may be responsible for the large off-track overpressures. The planforms with 62° and 70°leading edge sweep are shown in Figures 26a and 26b, respectively. The sweep of the outboard panel began at 57.5% and 34.06% span stations for the 62° and 70° sweep configurations, respectively. The shearing of the wing at 34% span resulted in a non-linear trailing edge of the wing. The planform area of the configuration with 70° sweep was increased slightly to maintain a bi-linear trailing edge. In addition to the sweep modifications, a nonlinear dihedral beginning at 57.5% of span which increases towards the tip was investigated for the Mach2 model. The dihedral near the tip was approximately 40°. The curve defining the dihedral is a monomial with an exponent of 10.0. The excessive dihedral was imposed in an attempt to move the peak overpressure beyond cutoff (approximately 55°). The results of these modifications at an azimuthal angle of 45° is shown in Figure 27a. The 62° swept wing reduced the peak overpressure by approximately 30% and the peak overpressure for the 70° swept wing was reduced by approximately 50%. The configuration with non-linear dihedral did not significantly change the on-or off-track pressure signatures of the original configuration. It is fortunate that the effect was small since the large dihedral would reduce the aerodynamic efficiency of the configuration. The effects of these design modifications on-ground-track are shown in Figure 27b. Note that there is little difference between the pressure signatures for the original model, wings with increased sweep, and non-linear dihedral. The configuration with 70° leading edge sweep has a larger expansion than the other configurations. This may be due to the modification of the 70 ° swept wing beginning at a more inboard station than the 62 swept wing.

CONCLUDING REMARKS

Euler CFD codes combined with extrapolation are capable of predicting pressure signatures for any azimuthal angle from centerline to near cutoff.

Euler CFD pressure signatures extrapolated from distances of approximately one quarter body length to experimental distances give acceptable correlations with experimental data. Good correlations also require the use of fine grids from the surface to the plane of the computational pressure signature, and reliable experimental data that is not contaminated by instrumentation and model support hardware should be available.

Dissipation in Euler codes used to facilitate convergence causes shocks to dissipate rapidly with increasing distance from the surface. Very fine grids are required even if the computations are taken near the model and extrapolated to experimental distances. The quality of the solution depends on grid density in the important regions of the flow field and the size of the computational space; the topology of the grid is of little importance.

The AIRPLANE unstructured grid generation program requires approximately one tenth of the time needed to generate a structured blocked grid for a complex configuration, but control of the point distribution is currently limited. For complete airplane configurations it is the only practical way to develop a grid.

Good experiment/CFD correlations have been achieved by performing the computations at a larger lift coefficient than the experimental value because of the lack of viscous decambering.

The limits on h/l for computing near-field pressure signatures needs further study. Dissipation, grid density, aspect ratio, and lift coefficient are important factors in determining such limits.

ACKNOWLEDGEMENT

The author would like to thank Tim Baker for his continued support and expertise in Computational Fluid Dynamics and grid generation, Scott Thomas for his expedient and efficient software development, Kurt Vaillancourt and Francis Enomoto for their CAD/CAM support.

REFERENCES

1. Mack, Robert J., and Needleman, Kathy E.: The Design of Two Sonic Boom Wind Tunnel Models from Conceptual Aircraft which Cruise at Mach Numbers of 2.0 and 3.0. AIAA paper No. 90-4026, 1990.

2. Haglund, George: HSCT Designs for Reduced Sonic Boom. AIAA paper No. 91-3103, Sept. 1991.

3. Cliff, Susan E., and Thomas, Scott D.: Euler/Experiment Correlations of Sonic Boom Pressure Signatures. AIAA -91-3276, Sept. 1991.

4. Cheung, S., Edwards, T., and Lawrence, S.: Application of CFD to Sonic Boom Near- and Mid-Field Prediction. AAIA-90-3999, 1990.

5 Madson, M.D.: Sonic Boom Predictions for Three Generic Models Using a Solution-Adaptive Full-Potential Code. AIAA-91-3278, 1991.

6. Siclari, M., and Darden, C.: CFD Predictions of the Near-Field Sonic Boom Environment for Two Low Boom HSCT Configurations. AIAA -91-1631.

7. Baker, Timothy J.: Automatic Mesh Generation for Complex Three-Dimensional Regions Using a Constrained Delaunay Triangulation. *Engineering with Computers 5*, 1989, pp. 161-175.

8. Baker, Timothy J.: Generation of Tetrahedral Meshes Around Complete Aircraft. 2nd international conference on numerical grid generation in computational fluid dynamics, Dec 5-8, 1988.

9. Baker, Timothy J.: Shape Reconstruction and Volume Meshing for Complex Solids. *International Journal for Numerical Methods in Engineering*, Vol. 32, 1991, pp.665-675 .

10. Jameson, A., and Baker, T.J.: Improvements to the Aircraft Euler Method. AIAA-87-0452, 1987.

11. Jameson, A.: A Vertex Based Multigrid Algorithm for Three Dimensional Flow Calculations. proceedings on numerical methods for compressible flows-Finite Difference and Volume Techniques, edited by T. E. Tezduar, and T. J. R. Hughes, AMD-vol 78, ASME, 1986, pp. 45-73.

12. Raj P., Olling, C.R., Sikora, J.S., Keen, J.M., Singer, S.W., and Brennan, J.E.: Three-dimensional Euler/Navier-Stokes Aerodynamic Method (TEAM). AFWAL-TR-87-3074, volumes 1-3, Dec., 1987.

13. Steinbrenner, John P., Chawner, John R., and Fouts, Chris L.: The Gridgen 3D Multiple Block Grid Generation System. WRDC-TR-90-3022, Volume 1, July, 1990.

14. Thomas, Charles: Extrapolation of Sonic Boom Pressure Signatures by the Waveform Parameter Method. NASA TN D-6832, 1972.

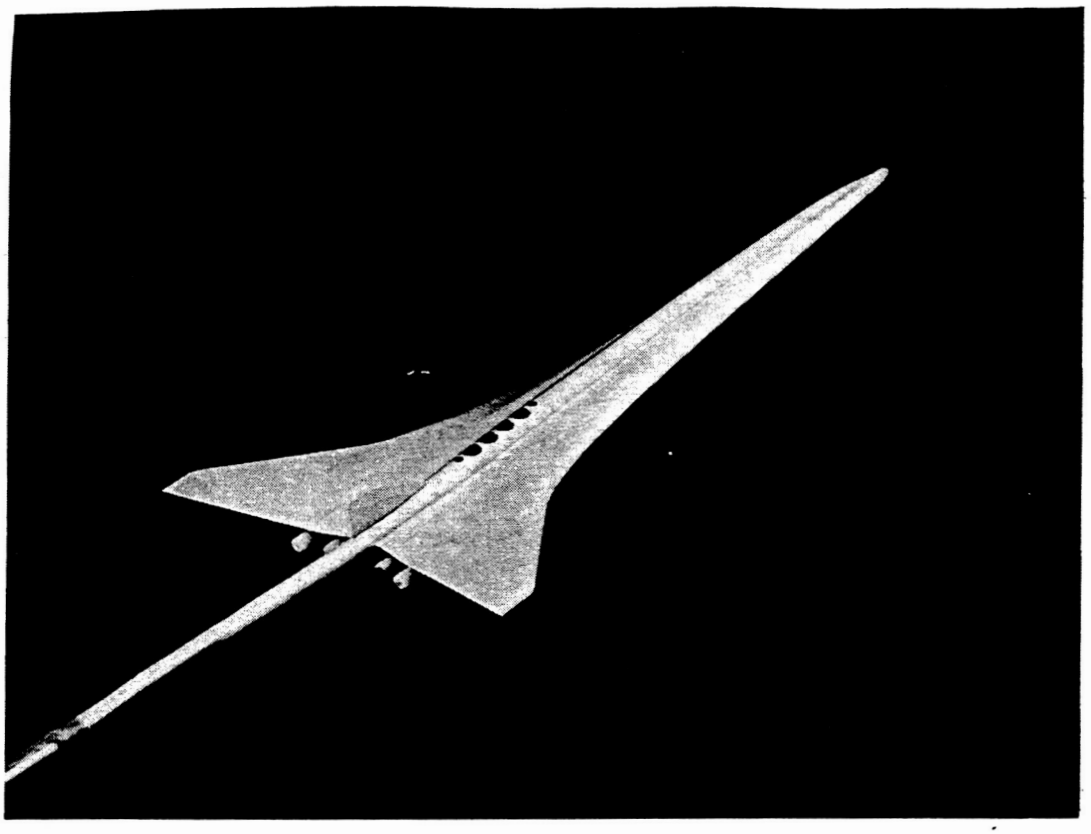

Figure 1. Photograph of the Mach2 configuration.

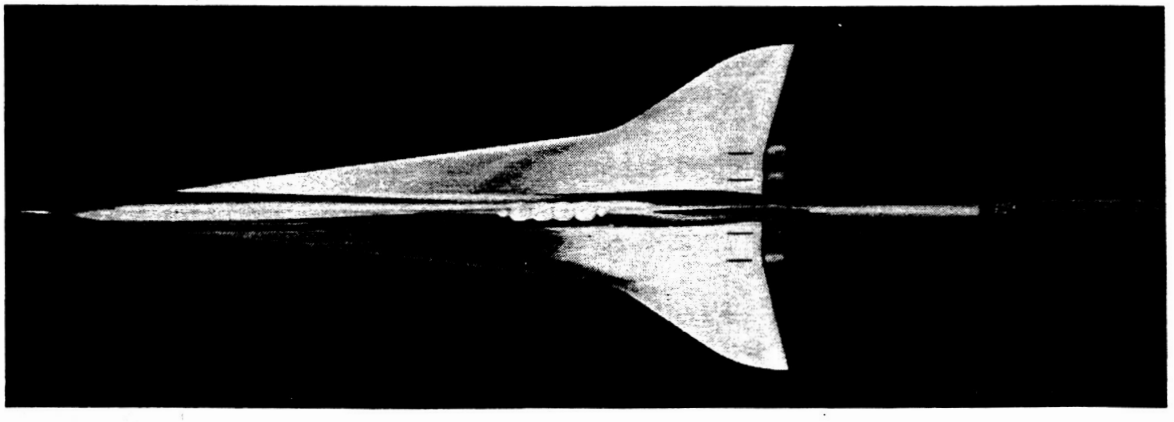

Figure 2. Photograph of the Mach3 configuration.

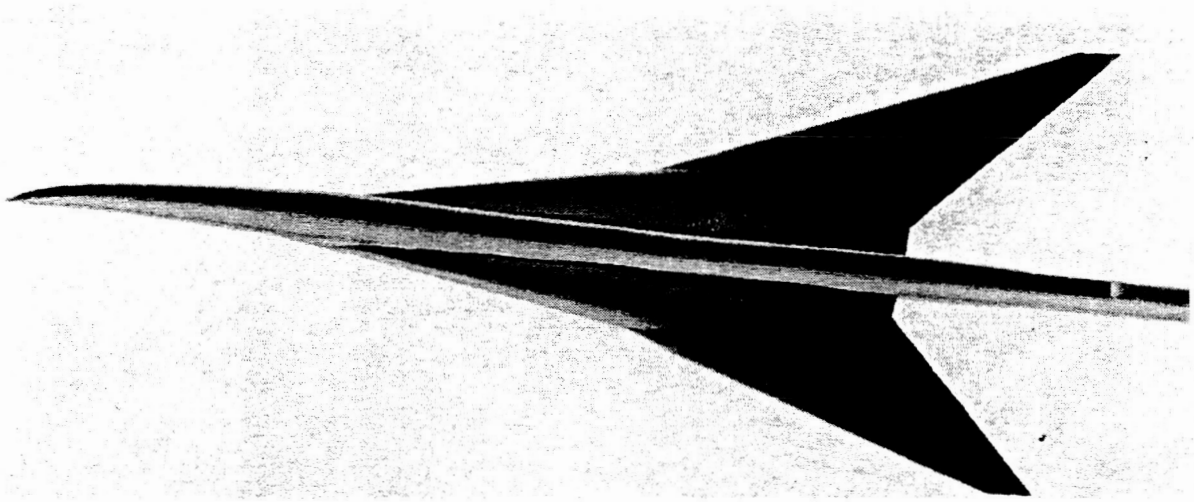

Figure 3. Isometric view of the Haglund Model, shaded by surface normals.

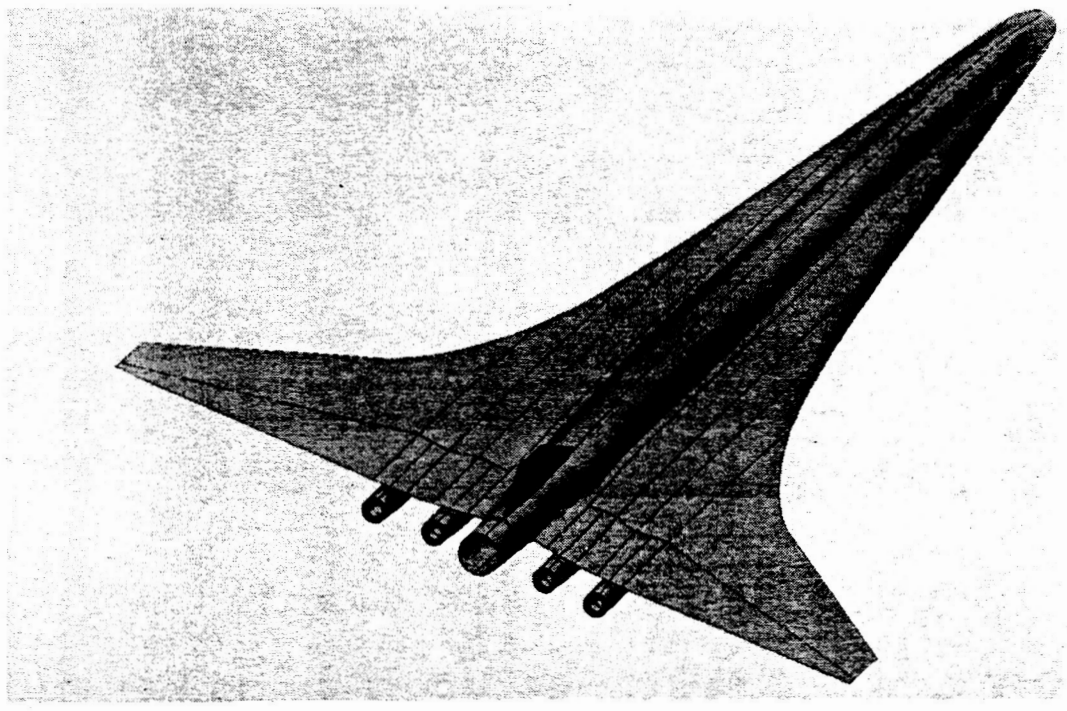

Figure 4. Computational grid with shaded surfaces showing the block boundaries of the multi-blocked grid.

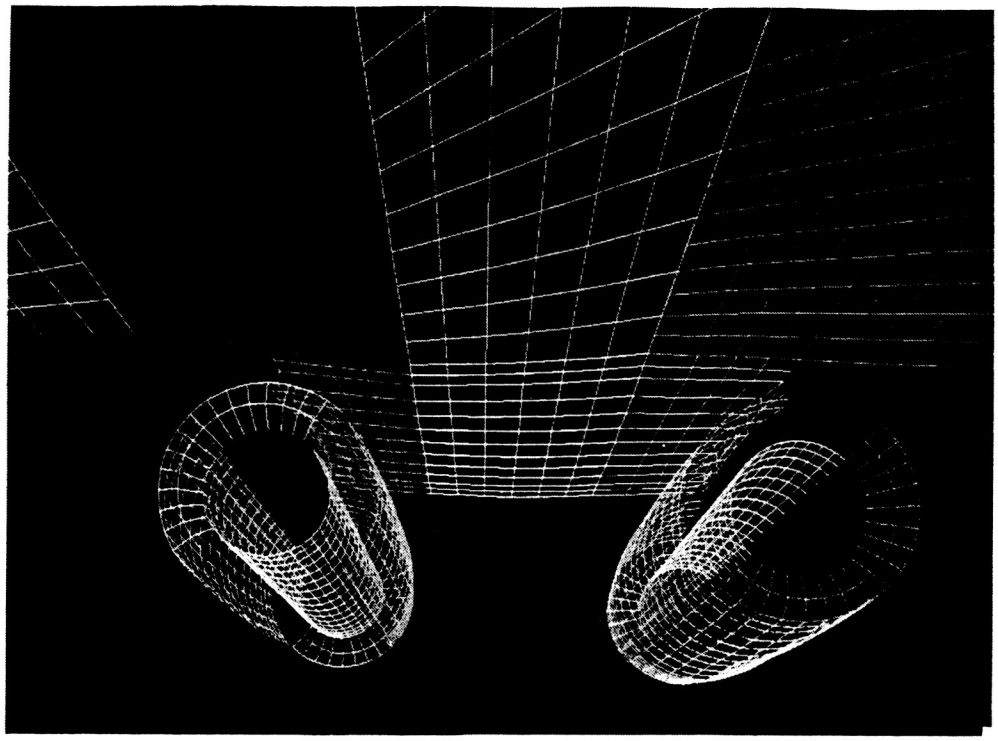

Figure 5. Lower surface view of the TEAM computational grid of the Mach2 computational grid showing the nacelles.

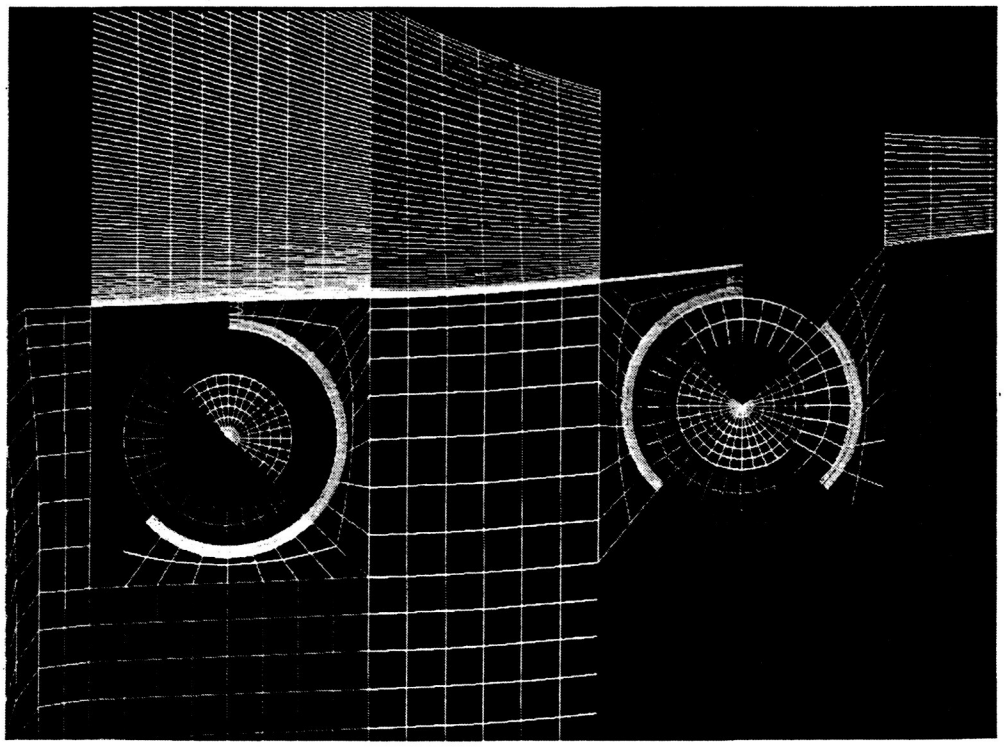

Figure 6. TEAM computational grid of the Mach2 configurations showing the grid plane at the inlet of the nacelle.

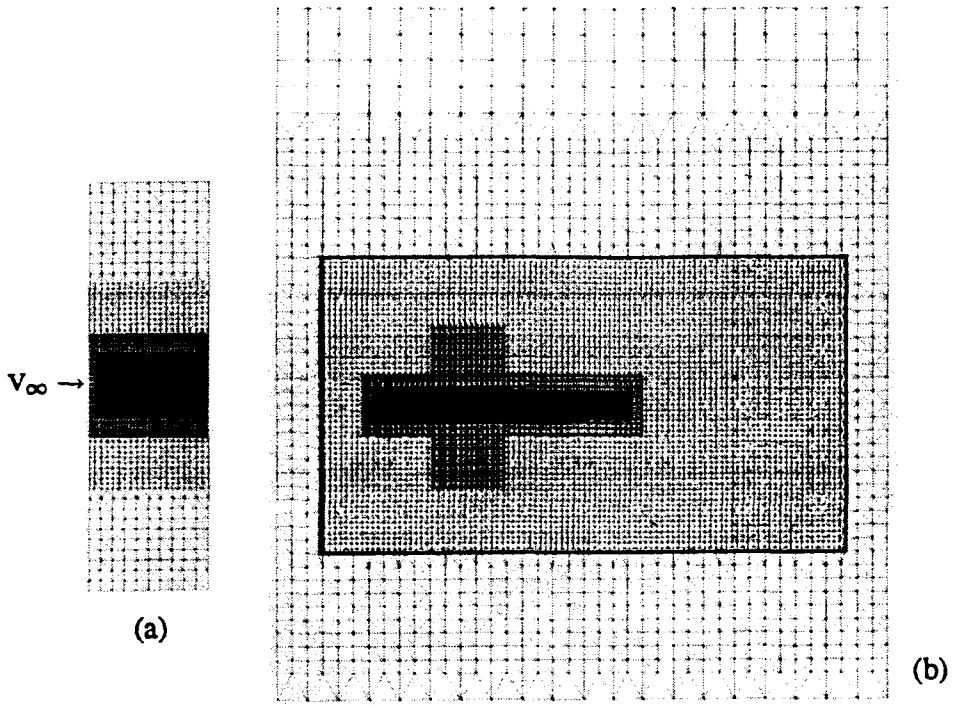

Figure 7. AIRPLANE unstructured grid for the Mach2 model.
(a) Entire centerplane.
(b) Expanded view of centerplane.

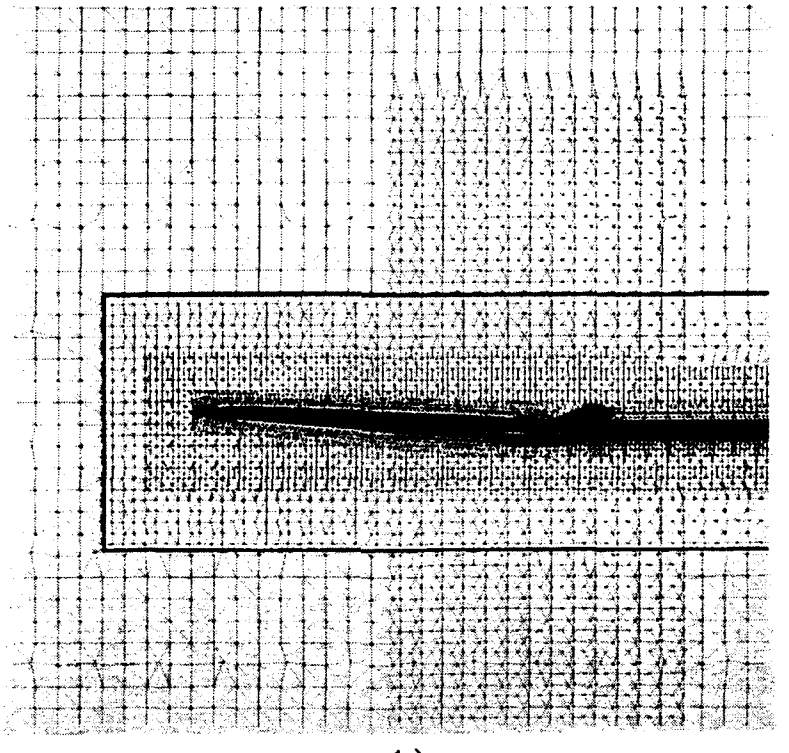

7 (c) Expanded view of centerplane.

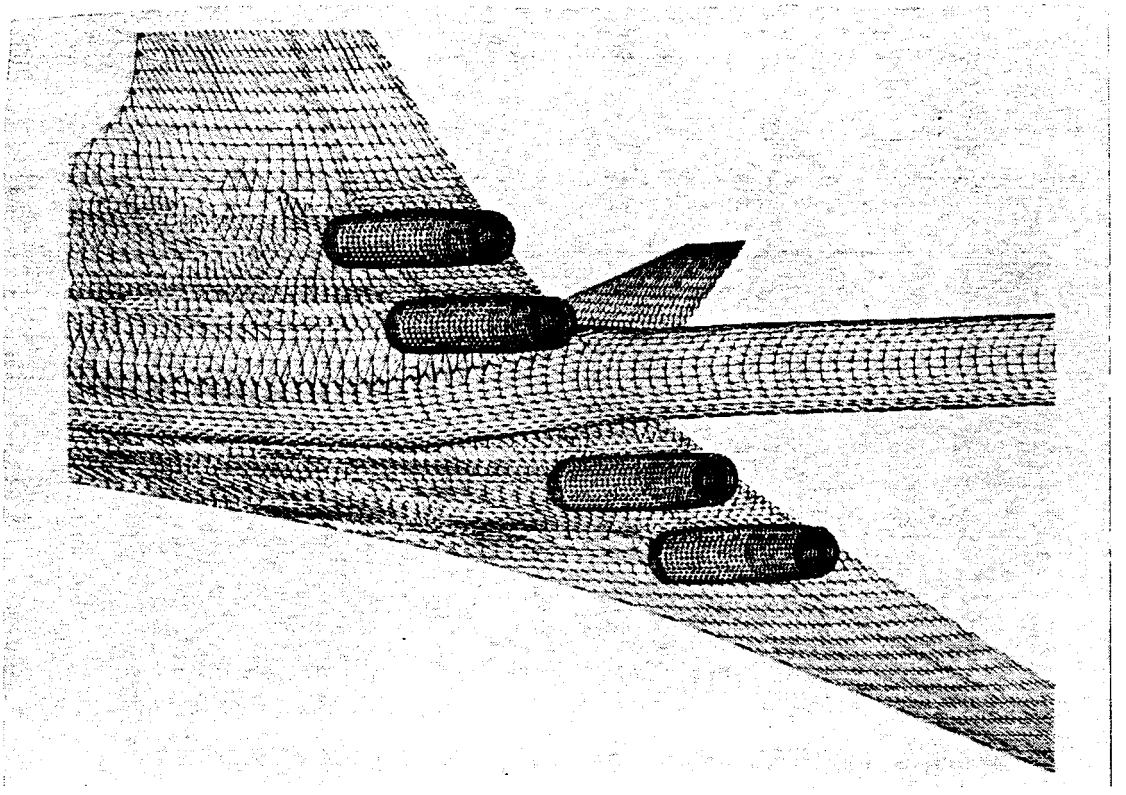

Figure 8. Lower surface of the Mach2 configuration with flow-through nacelles.

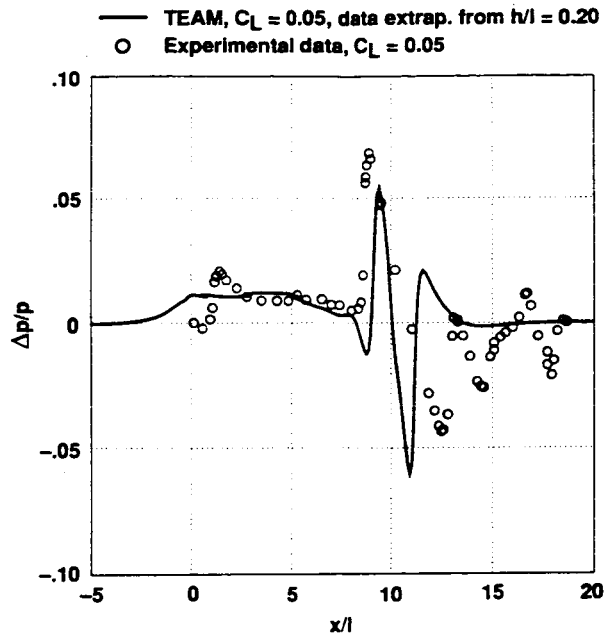

Figure 9. Pressure signatures for the Mach2 model with flow-though nacelles, M = 2.0, h/l = 1.085.

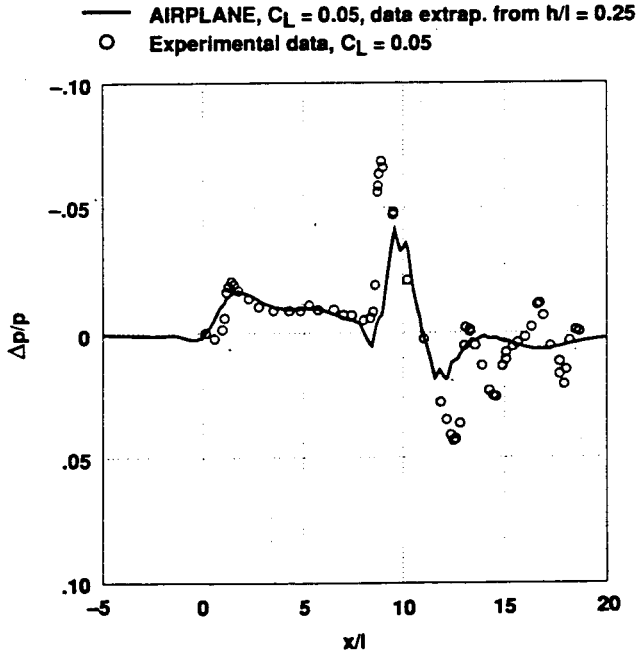

Figure 10. Pressure signatures for the Mach2 model with flow-though nacelles, M =2.0, C_L = 0.065, h/l = 1.085.

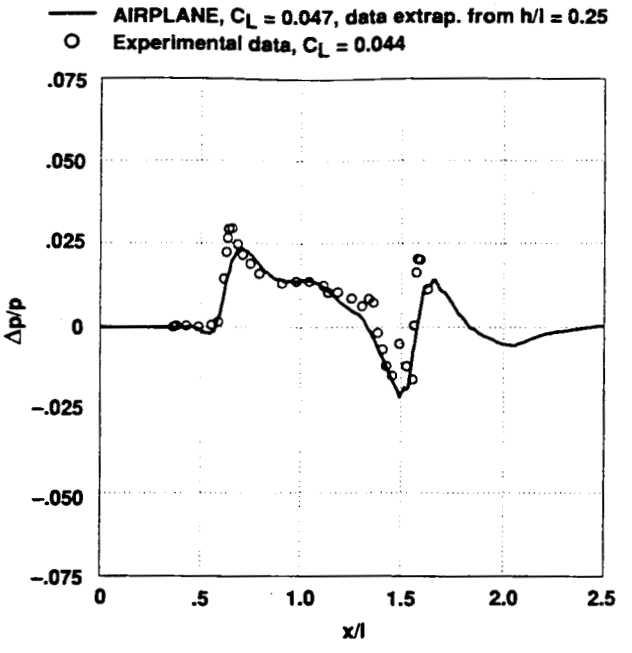

Figure 11. Pressure signatures for the Mach2 model without nacelles, M = 2.0, ϕ = 0.0°, h/l = 0.66.

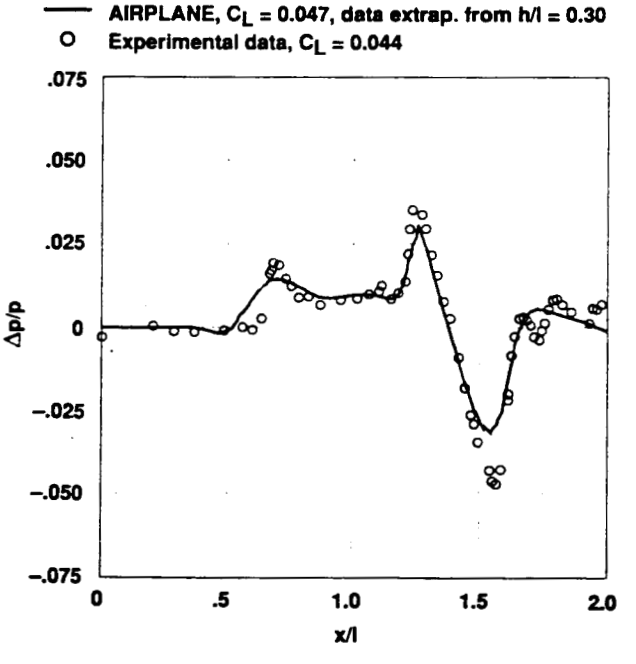

Figure 12. Pressure signatures for the Mach2 model without nacelles, M = 2.0, ϕ = 45.0°, h/l = 0.66.

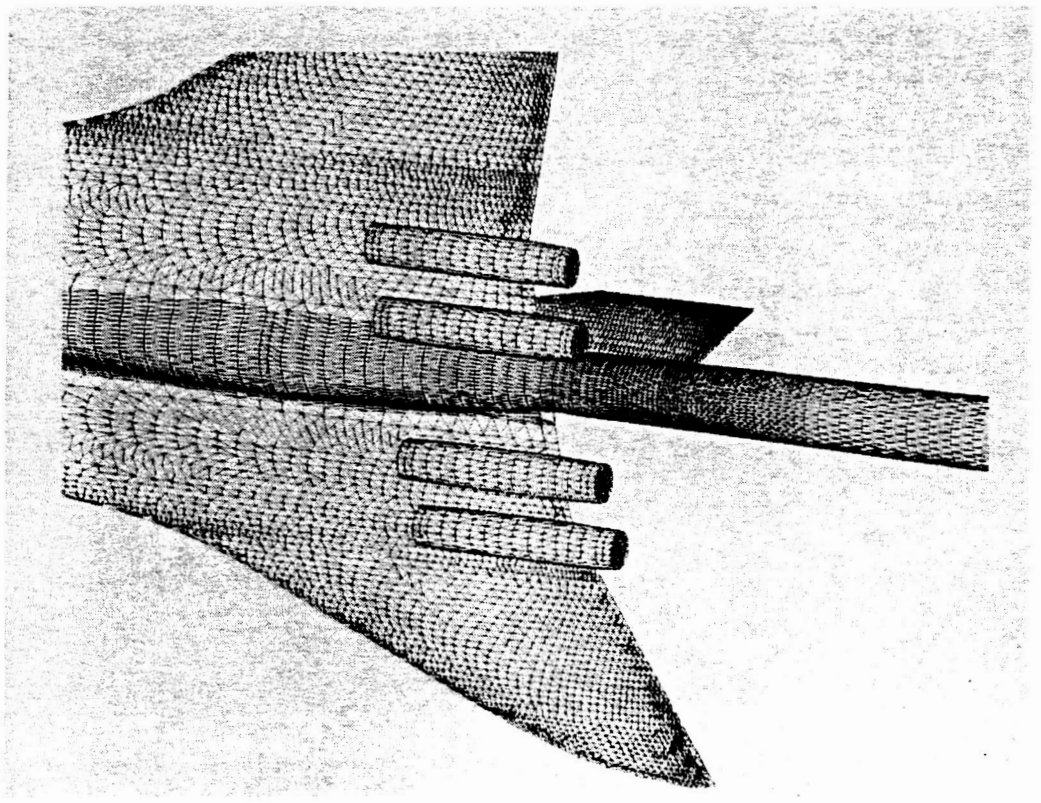

Figure 13. Lower surface of the Mach3 configuration with blocked nacelles.

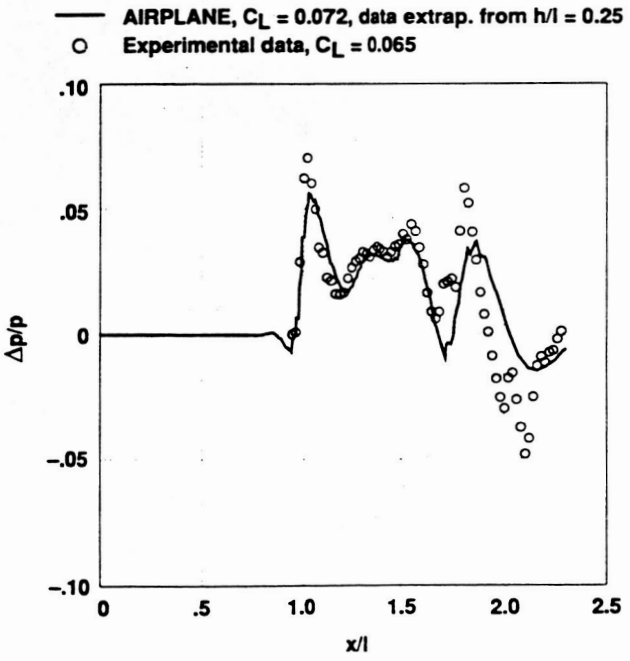

Figure 14. Pressure signatures for the Mach3 model, M = 2.50, ϕ = 0.0°, h/l = 0.47.

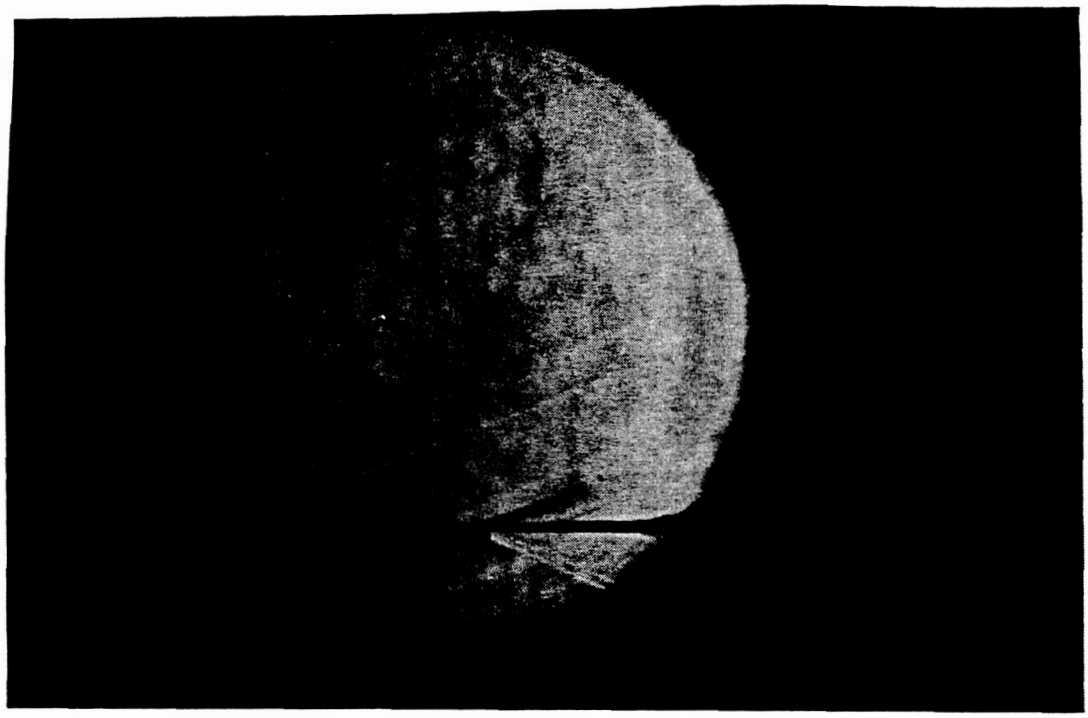

Figure 15. Schlieren photograph of the Mach3 model in the Ames 9x7 Supersonic Wind Tunnel, M = 2.5, $\alpha = 2.0°$.

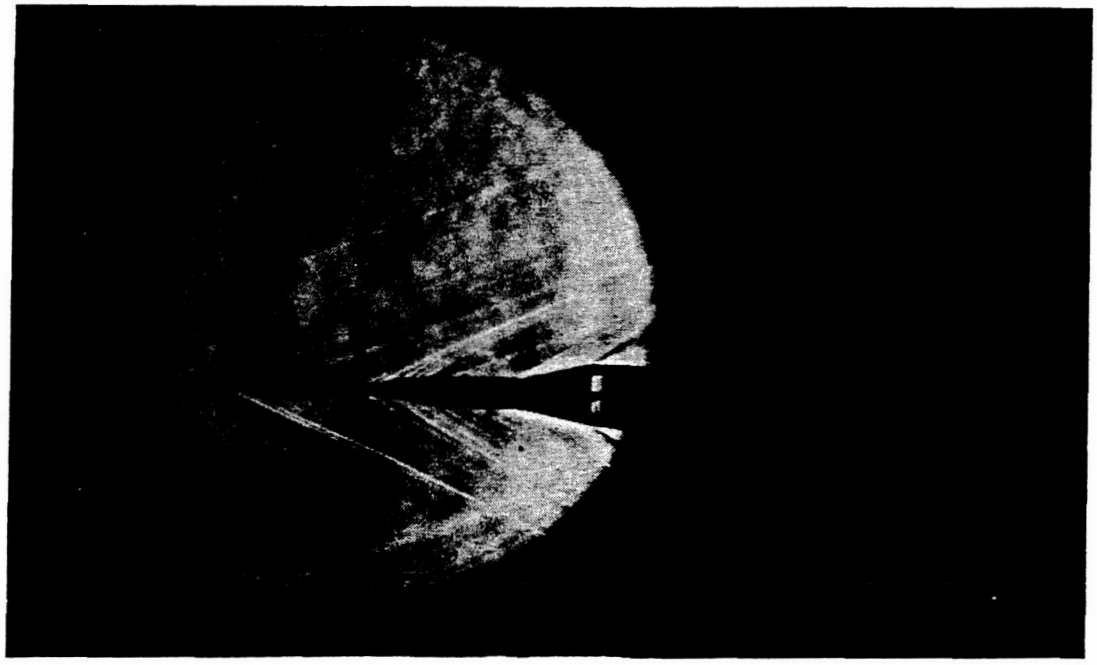

Figure 16. Schlieren photograph of the aft portion of the Mach3 model, sting and angle of attack mechanism in the Ames 9x7 Supersonic Wind Tunnel.

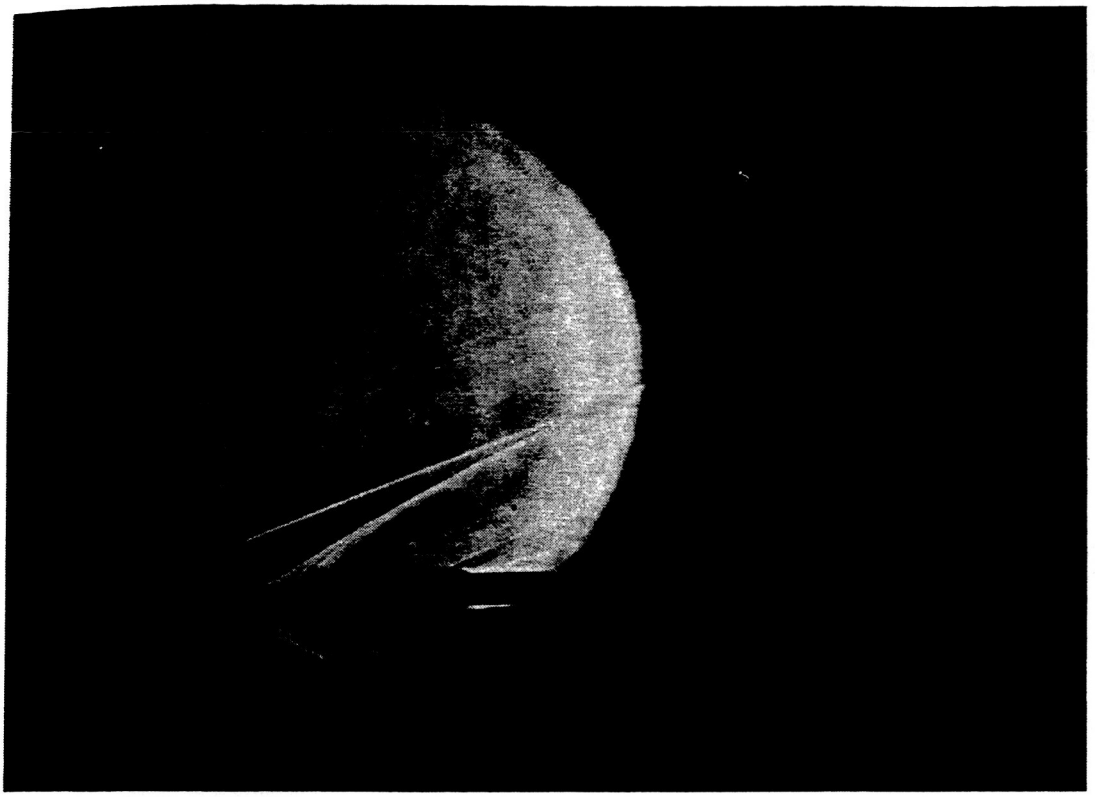

Figure 17. Schlieren photograph of the angle of attack mechanism in the Ames 9x7 Supersonic Wind Tunnel.

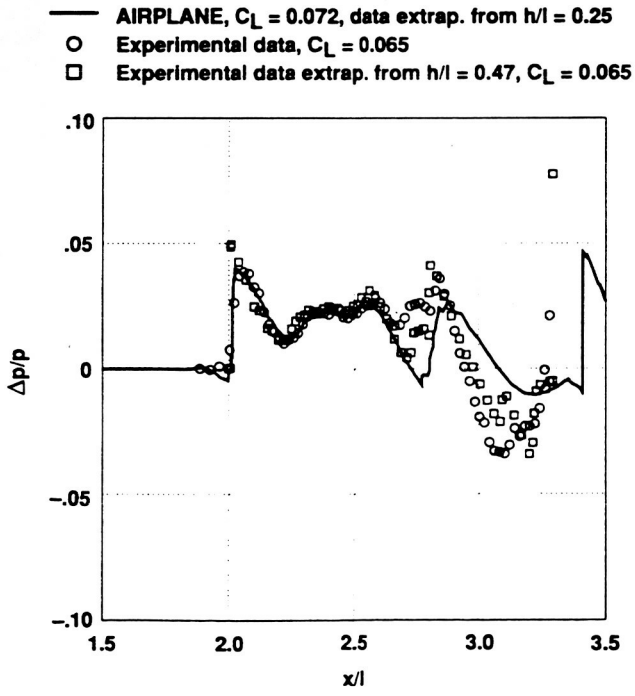

Figure 18. Pressure signatures for the Mach3 model without nacelles, M = 2.50, ϕ = 0.0°, h/l = 0.94.

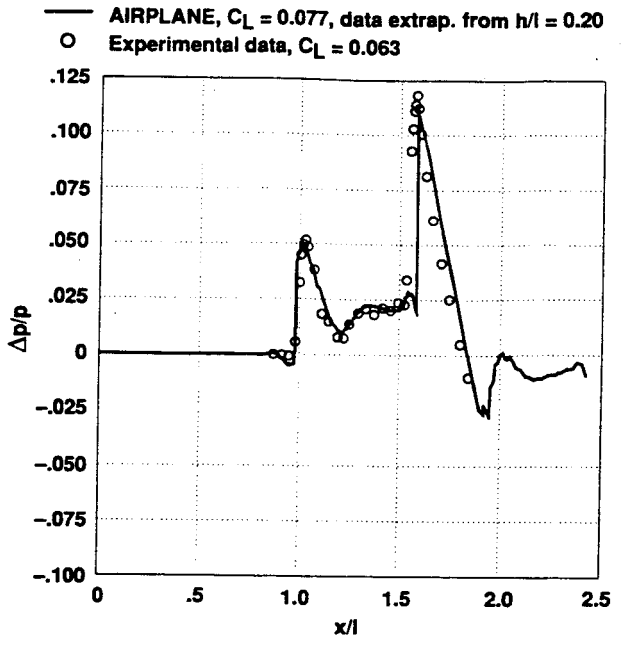

(a) h/l = 0.68.

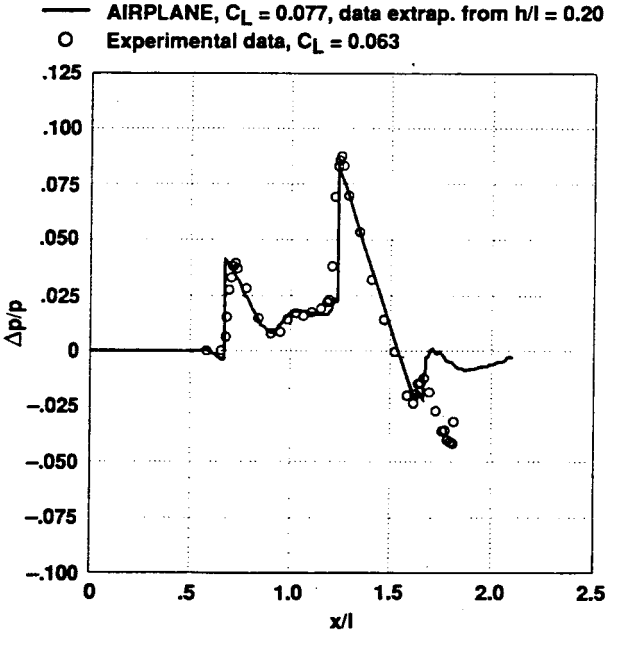

(b) h/l = 1.01.

Figure 19. Pressure signatures for the Mach3 model with blocked nacelles, M = 2.50, $\phi = 0.0°$.

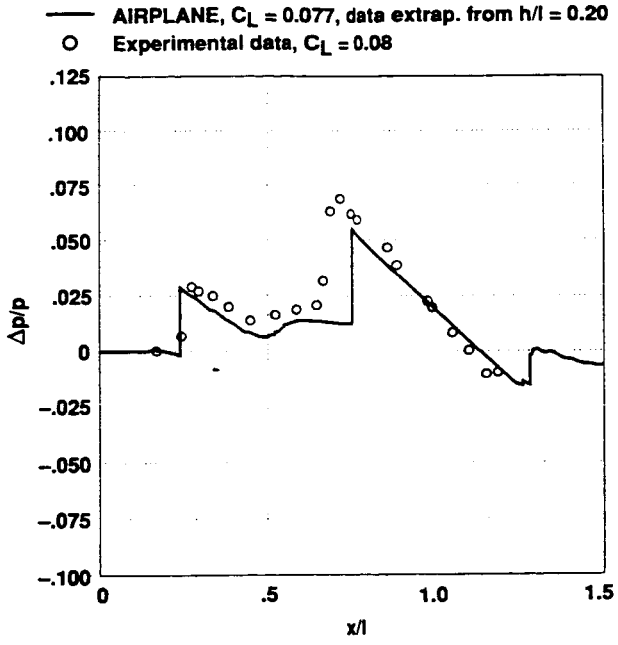
AIRPLANE, C_L = 0.077, data extrap. from h/l = 0.20
Experimental data, C_L = 0.08
.125
.100
.075
.050
.025
0
–.025
–.050
–.075
–.100
Δp/p
0
.5
1.0
1.5
x/l

19(c) h/l = 1.81.

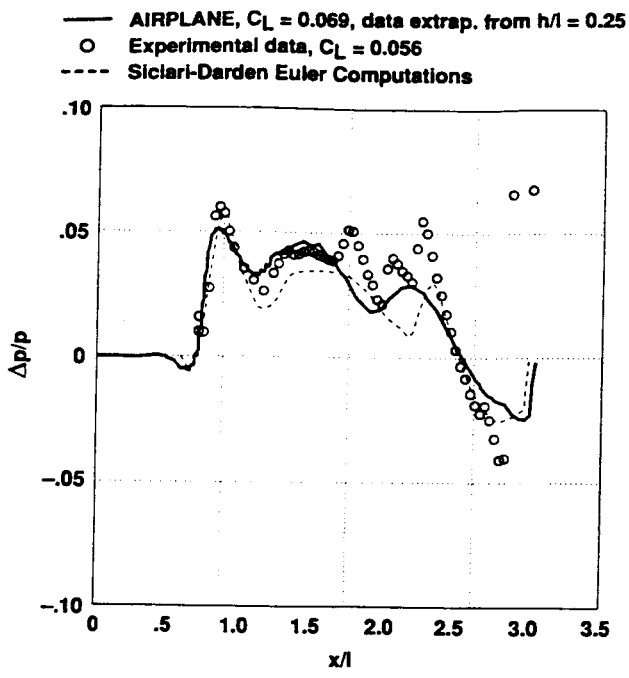

(a) h/l = 0.67.

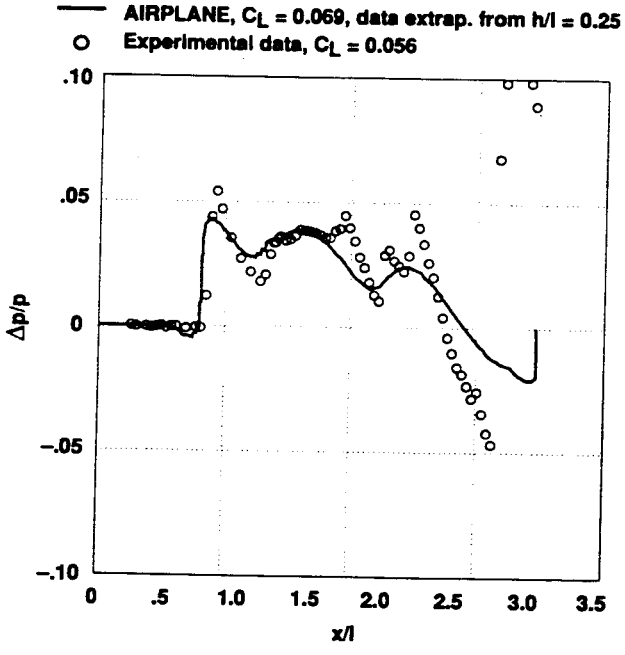

20(b) h/l = 0.94.

Figure 20. Pressure signatures for the Mach3 model without nacelles, M = 2.96, ϕ = 0.0°,

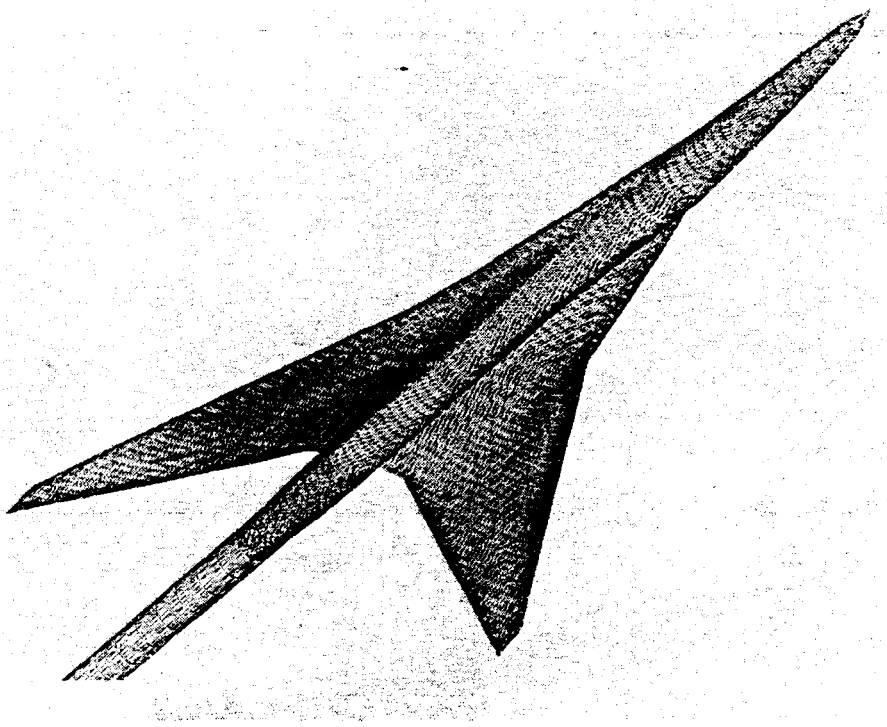

Figure 21. Isometric view of the upper surface unstructured computational grid for the Haglund model without nacelles.

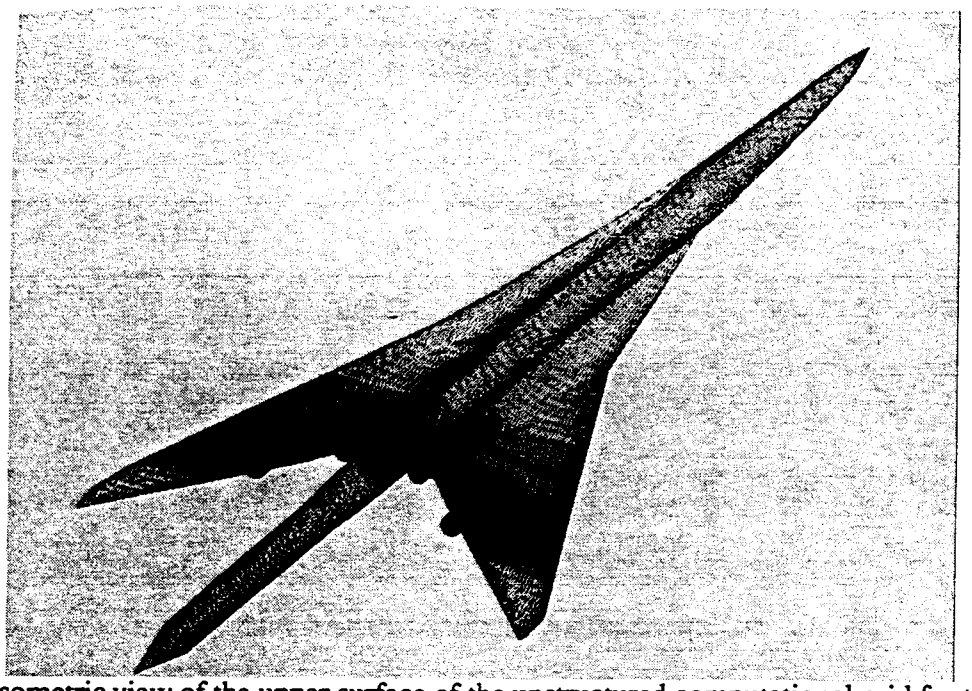

Figure 22. Isometric view of the upper surface of the unstructured computational grid for the Haglund model with nacelles and diverter.

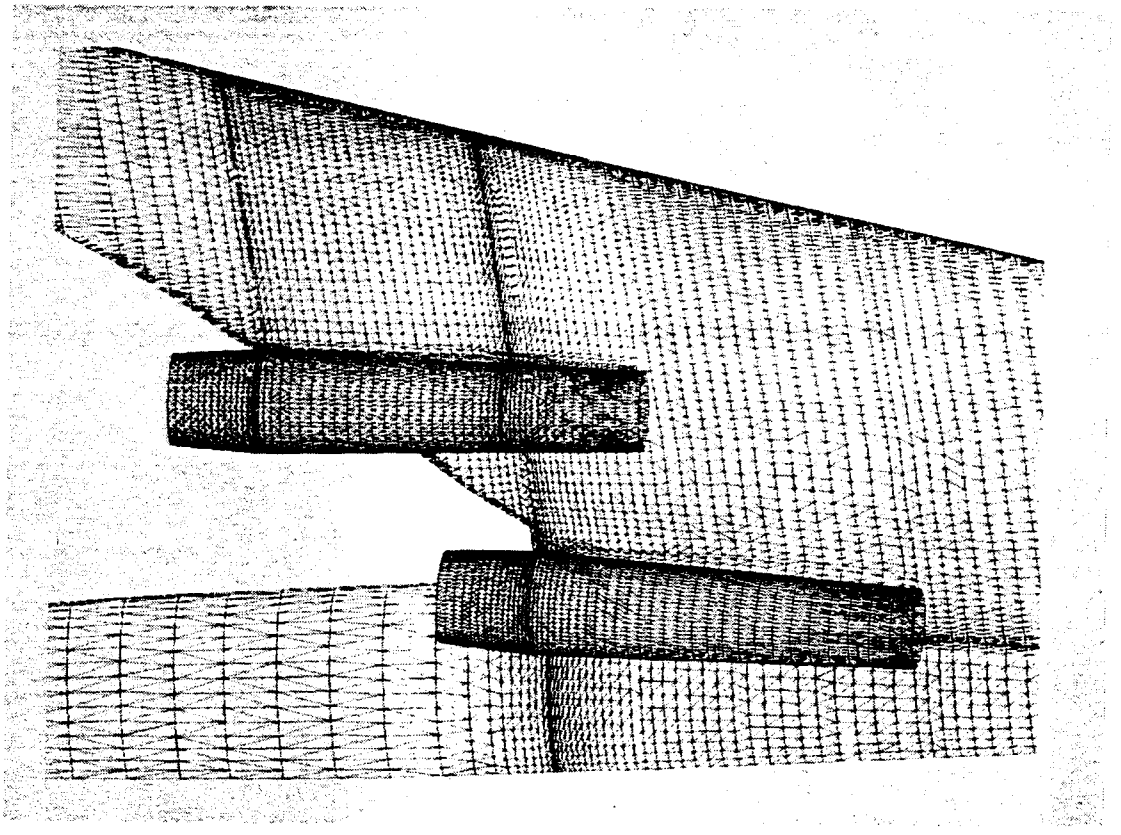

Figure 23. Isometric view of the lower surface of the unstructured computational grid for the Haglund model with nacelles and diverter.

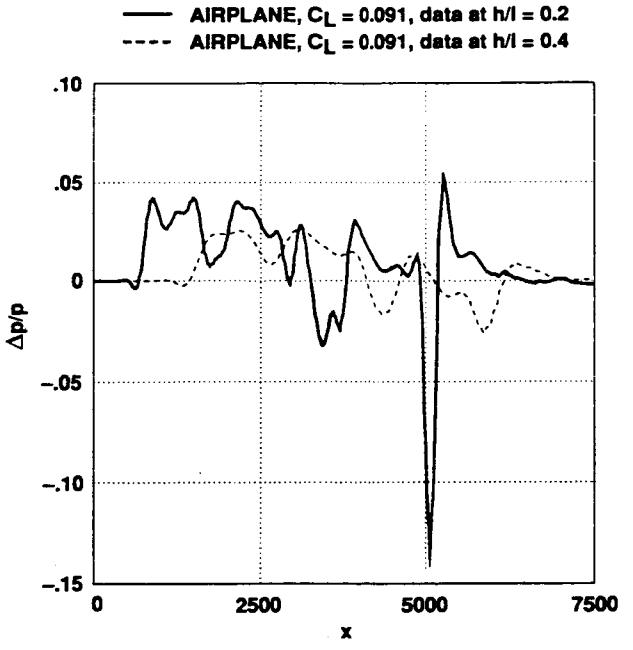

Figure 24. Pressure signature for the Haglund model without nacelles, M = 1.70, ϕ = 0.0°.

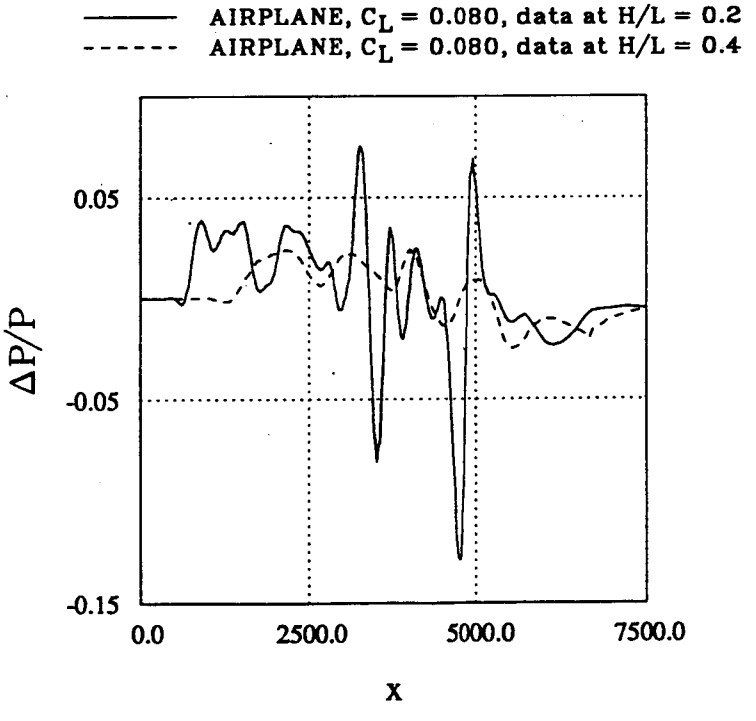

Fig. Pressure Signatures for the Haglund model with diverters and nacelles, M = 1.70, ϕ = 0

Figure 25. Pressure signature of the Haglund model with nacelles and diverters modeled, M = 1.70, ϕ = 0.0°.

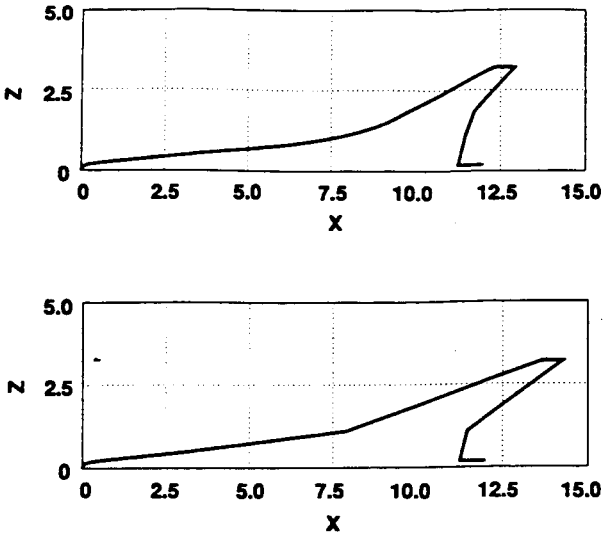

Figure 26. Modified Mach2 Models.
(a) 62° outboard sweep.
(b) 70° outboard sweep.

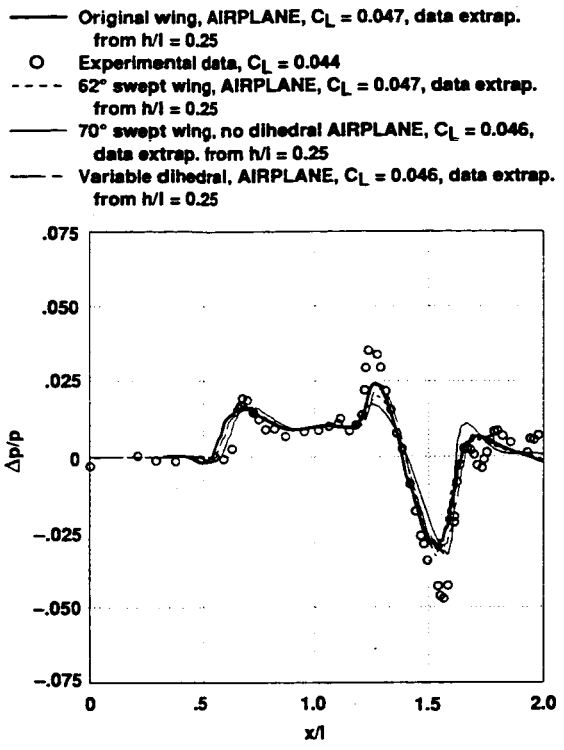

(a) h/l = 0.067.

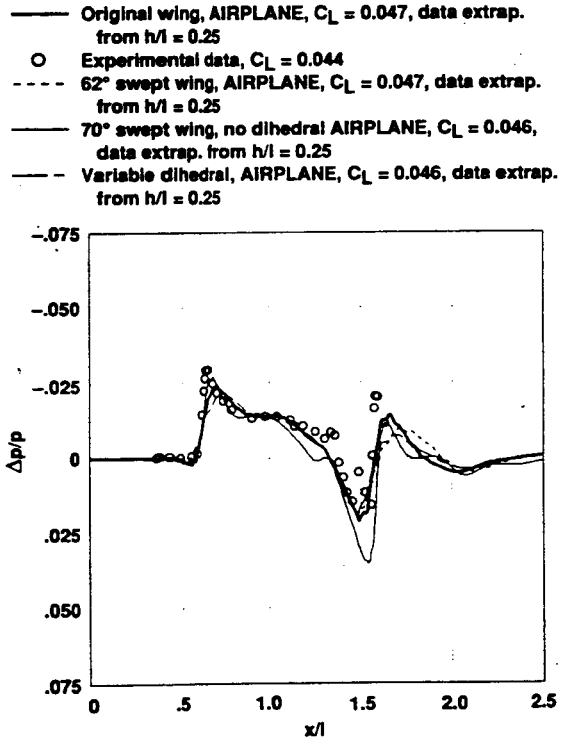

(b) h/l = 0.66.

Figure 27. Pressure signatures for the Mach2 and modified Mach2 models without nacelles, M = 2.0, ϕ = 45.0°.